Journal of Vibration Engineering & Technologies (2024) 12:7847–7865
https://doi.org/10.1007/s42417-024-01331-1

ORIGINAL PAPER

Electromechanical Vibration Response of Pre-stressed Bi-layered Piezoelectric Plate Under a Harmonic Mechanical Force

Ahmet Daşdemir[1]

Received: 28 May 2023 / Revised: 20 September 2023 / Accepted: 26 February 2024 / Published online: 2 April 2024

Abstract

Purpose This study presents the outcomes of a finite element analysis (FEA) of forced vibrations by a time-harmonic loading of a bi-layered piezoelectric plate with two-axially pre-stressed layers.

Methods The investigation is conducted based on the following assumptions: (i) the resultant system is resting on a rigid foundation, (ii) each layer is poled along the direction perpendicular to the free surface, (iii) a complete contact state exists at the interface of the plane in the plate, and (iv) the initial stress state at the layers is modeled based on the three-dimensional linearized theory of elasticity for solids under initial stress (TLTESIS). First, we describe nonlinear governing equations of motion and boundary-contact conditions for the dynamical model of the current system and then apply a linearization and non-dimensionalization procedure to the problem under consideration. In terms of Hamilton principle, a finite element model (FEM) is developed based on the weak form.

Results and Conclusions The proposed and validated FEM approach can help to address several issues in the piezoelectric structure of finite lengths, either pre-stressed or not. In particular, we present an investigation of the effects of changing problem factors on the dynamic behavior as well as the frequency response of the composite plate. The numerical results demonstrate that the stress transition across the interface of the layers plays a key role in the resonance mode of the system, in both a quantitative sense and a qualitative sense.

Keywords Forced vibration · Bi-layered plate · Piezoelectric material · Finite element method · Two-axially initial stress

Introduction

The production process of engineering structures has always been an important step for designers. Structural vibrations in a medium are now an active area of research. In particular, it was realized in the 1880s that some solids called piezoelectric materials display electrical effects against changes from external factors. This interesting property gives a wide opportunity for researchers to do many potential practices of these materials in daily life and engineering applications, such as electricity generation, energy harvesting, smart systems, sensors, isolation of acoustics/radiation, and air conditioning systems. Recently, there is a growing interest in the study of piezoelectricity, attracting more and more scientists' attention to improve many engineering systems. For more details on the historical backgrounds and mechanical properties of the piezoelectric materials, one may read the references in [1–3].

When a solid is exposed to a force, a nonlinear wave distribution generally appears in the medium. Therefore, describing and solving perturbations in the body could mathematically be impossible sometimes. Many researchers have made some studies in the past to overcome this difficulty. In the early XXth century, British mathematician Sir Richard Vynne Southwell presented the first serious theoretical approach to the subject [4]. Hence, a theory that is so-called Three-Dimensional Linearized Equations (TDLE) was laid down. Adhering to the fundamental principle of the TDLE, the development process of this theory was continued by Biezeno and Henky [5] and was accelerated by Biot [6], Neuber [7], Green [8], Guz [9], Tiersten [10], Hoger [11], Ogden [12], and Reddy [13] due to some reasons such as problem geometry, deformation type, and material design.

Based on the above-stated requirements, many mechanical problems in various configurations and effects of respective

✉ Ahmet Daşdemir
ahmetdasdemir37@gmail.com

[1] Department of Mathematics, Faculty of Science, Kastamonu University, Kastamonu, Turkey

factors were explored by a great number of scientists. Here, some remarkable ones can be remembered. Wang and Zhao presented a formulation of a dynamic problem related to the propagation of the Love wave in a piezoelectric layer on the elastic substratum with interfacial defect [14]. Yu and Zhang analyzed the guided wave propagation in FGM plates under gravity and various initial stress states according to the mechanics of incremental deformations [15]. Rouzegar and Abad focused on free vibration analysis of composite plates integrated with piezoelectric faces within the scope of the four-variable refined plate theory [16]. Kurt et al. [17] investigated the effect of the initial stresses on the Lamb wave propagation in a pre-stressed sandwich plate with a metal elastic core bonded perfectly to piezoelectric faces. Daşdemir [18] modeled forced vibration analysis of a pre-stressed sandwich plate-strip consisting of elastic faces imperfectly bonded to a piezoelectric core. Duc et al. [19] analyzed the nonlinear dynamic response of higher-order shear deformable sandwich functionally graded circular cylindrical shells with piezoelectric actuators under the influence of thermo-electro-mechanical and damping loads. Kumar et al. [20] considered the propagation of shear waves in a composite structure with a piezoelectric layer resting on a micro-polar half space for an imperfect contact case. Kumar et al. [21] studied the dynamic behavior of horizontally polarized shear (SH) waves in an imperfectly bonded functionally graded piezoelectric material layer resting on a functionally graded porous piezoelectric material half-space. Shahdadi and Rahnama [22] presented an analytical solution for the free vibration behavior of functionally graded (FG) annular sector plates integrated with piezoelectric layers using Hamilton's principle and Maxwell's electrostatic equation. Chan et al. [23] analyzed the free vibration problem in a functionally graded porous (FGP) truncated conical panel with piezoelectric actuators in thermal environments resting on the Winkler–Pasternak foundation. Sahu et al. [24] reported the reflection and transmission phenomena of plane waves through the interface of two piezoelectric semiconductor half-spaces with initial stresses. Pankov [25] studied the effective modulus problem of statistical mechanics of a pre-stressed piezo-active composite using the Green function method. Othmani and Khelfa [26] investigated the guided wave propagation in functionally graded piezoelectric-piezomagnetic (FGPP) plates with negative magnetic permeability using a Legendre polynomial method.

There is a noteworthy investigation factor in the above-stated problems, i.e., the initial stress state in materials. The initial stress state in a mechanical system increases the nonlinearity degree of wave propagations. Many efforts were made in the past to overcome this difficulty. In this paper, we will utilize the three-dimensional linearized theory of elasticity for solids under initial stress (TLTESIS) developed by Ukrainian mechanical scientist Guz [27] to eliminate the nonlinearity caused by the initial stress state. More detailed information about this theory can be obtained from the monograph by Akbarov [28]. Within the scope of TLTESIS, a great number of papers paid attention to mechanical investigations. Ilhan focused on the dynamical behavior of a pre-stressed system of an infinite plate-strip and a half-plane under a moving time-harmonic load [29]. Negin et al. [30] analyzed the effect of imperfect contact interaction in the tangential direction on the dispersion relation of the generalized Rayleigh waves in a pre-stressed system of a covering layer and a half-plane. Daşdemir and Eröz [31] solved numerically the forced vibration problem in an elastic two-layered plate-strip of initial stress with finite length. Yesil [32] considered forced and natural vibration problems in a rectangular pre-stressed orthotropic composite plate of two parallel cylindrical cavities with rounded-off corners. Glukhov [33] solved the problem of axisymmetric wave propagation in a composite material of two incompressible alternating types of layers with initial stresses. Daşdemir [34] presented a three-dimensional finite element model for studying the dynamic response of pre-stressed bi-layered elastic plate resting on a rigid foundation. Akbarov and Bagirov [35] investigated propagation of the axisymmetric waves in the pre-strained highly elastic plate in contact with a compressible inviscid fluid.

As the above brief literature review reveals, modeling forced vibrations of a pre-stressed bi-layered piezoelectric plate subjected to a time-harmonic force resting on a rigid ground has yet to receive attention. Hence, a key attention was paid to the dynamic response of the body in the present study. According to the fundamental principles of TLTESIS, the formulation of the dynamic problem under consideration is constructed, and the equations of motion and related boundary-contact conditions are derived in the plane-strain state. The investigation is carried out under the assumptions that there are rigidly clamped cases at interfaces between the layers and that each layer is polled in parallel to the external force. Next, a solution procedure related to governing equations of motion is designated using the finite element method (FEM) based on the variational calculus and the virtual work principle. In particular, numerical results related to the influence of problem parameters on the frequency response of the plate are presented.

The rest of the manuscript is organized as follows. "Statement of the Problem" section structurally introduces the dynamical stress field problem regarding our model while "Solution Procedure" section displays the three-dimensional finite element model. "Numerical Results and Discussions" section is divided into two parts. In the first part, the accuracy and convergence of the proposed solution procedure is proven, and following this, some numerical concrete examples are given. In the last section, we summarize and discuss some concluding remarks for our numerical results.

Statement of the Problem

Let us consider a bi-layered piezoelectric plate, resting on a rigid foundation, occupying the three-dimensional domain V of a right rectangular prism bounded by a surface Γ of six planes. A Cartesian coordinate system is applied to the plate corner on the top surface. The system under consideration is of the size of length $2a_1$ in the x_1-direction, width $2a_3$ in the x_3-direction, and total thickness h in the x_2-direction whose configurations are shown in Fig. 1. In addition, whereas the upper layer's thickness is h_1, the lower layer's is h_2. To distinguish the quantities of the layers, the superscript "(m)" is used.

The coupled electro-elastic constitutive relations were given by Tiersten [36] as

$$\sigma_{ij}^{(m)} = c_{ijkl}^{(m)} S_{kl}^{(m)} - e_{ijk}^{(m)} E_k^{(m)},\ D_i^{(m)} = e_{ikl}^{(m)} S_{kl}^{(m)} + \gamma_{ik}^{(m)} E_k^{(m)},$$

where $i, j, k, l = 1, 2, 3$ and $m = 1, 2$. To be clear, these are fourth- and third-rank tensors. For the current analysis, it is assumed that each layer of the plate is polled perpendicular to the top surface. In this case, by the proper tensor transformation, the stress–strain relations can be given explicitly as follows [2]:

$$\begin{Bmatrix} \sigma_{11} \\ \sigma_{22} \\ \sigma_{33} \\ \sigma_{12} \\ \sigma_{23} \\ \sigma_{31} \end{Bmatrix}^{(m)} = \begin{bmatrix} c_{11} & c_{13} & c_{12} & 0 & 0 & 0 \\ c_{13} & c_{33} & c_{13} & 0 & 0 & 0 \\ c_{12} & c_{13} & c_{11} & 0 & 0 & 0 \\ 0 & 0 & 0 & c_{44} & 0 & 0 \\ 0 & 0 & 0 & 0 & c_{44} & 0 \\ 0 & 0 & 0 & 0 & 0 & c_{66} \end{bmatrix}^{(m)} \begin{Bmatrix} S_{11} \\ S_{22} \\ S_{33} \\ 2S_{12} \\ 2S_{23} \\ 2S_{31} \end{Bmatrix}^{(m)} - \begin{bmatrix} 0 & e_{31} & 0 \\ 0 & e_{33} & 0 \\ 0 & e_{31} & 0 \\ 0 & 0 & e_{15} \\ 0 & 0 & 0 \\ e_{15} & 0 & 0 \end{bmatrix}^{(m)} \begin{Bmatrix} E_1 \\ E_2 \\ E_3 \end{Bmatrix}^{(m)}, \tag{1}$$

$$\begin{Bmatrix} D_1 \\ D_2 \\ D_3 \end{Bmatrix}^{(m)} = \begin{bmatrix} 0 & 0 & 0 & 0 & 0 & e_{15} \\ e_{31} & e_{33} & e_{31} & 0 & 0 & 0 \\ 0 & 0 & 0 & e_{15} & 0 & 0 \end{bmatrix}^{(m)} \begin{Bmatrix} S_{11} \\ S_{22} \\ S_{33} \\ 2S_{12} \\ 2S_{23} \\ 2S_{31} \end{Bmatrix}^{(m)} + \begin{bmatrix} \gamma_{11} & 0 & 0 \\ 0 & \gamma_{33} & 0 \\ 0 & 0 & \gamma_{11} \end{bmatrix}^{(m)} \begin{Bmatrix} E_1 \\ E_2 \\ E_3 \end{Bmatrix}^{(m)}, \tag{2}$$

where $\sigma_{ij}^{(m)}$, $D_i^{(m)}$, $S_{ij}^{(m)}$, and $E_i^{(m)}$ are the stress, electric displacement, strain, and electric field components, respectively; $c_{ij}^{(m)}$, $e_{ij}^{(m)}$, and $\gamma_{ij}^{(m)}$ are elastic, piezoelectric, and permittivity coefficients, respectively. The linear strain–displacement and the electric field-potential relations are defined by

$$S_{ij}^{(m)} = \frac{1}{2}\left(\frac{\partial u_i^{(m)}}{\partial x_j} + \frac{\partial u_j^{(m)}}{\partial x_i} \right) \quad \text{and} \quad E_i^{(m)} = -\varphi_{,i}^{(m)}, \tag{3}$$

where $u_i^{(m)}$ and $\varphi^{(m)}$ are the displacement and electrical potential components.

The production process of the plate is encapsulated as follows. First, the lateral surfaces of each layer are individually exposed to a static normal (tension or compression) force, in both horizontal directions. This also yields initial electrical displacements in the layers linearly in proportional to mechanical impact. From Eqs. (1) and (2), the following relations are directly obtained [37]:

$$D_1^0 = \frac{e_{33}(c_{11}+c_{12}) - 2c_{13}e_{31}}{c_{33}(c_{11}+c_{12}) - 2(c_{13})^2} \sigma_{11}^0 \Big|^{(m)} \quad \text{and}$$

$$D_3^0 = \frac{(c_{11}-2c_{12}+c_{22})c_{13}e_{31} + (c_{12}^2 - c_{11}c_{22})e_{33}}{(c_{11}-2c_{12}+c_{22})c_{13}^2 + (c_{12}^2 - c_{11}c_{22})c_{33}} \sigma_{33}^0 \Big|^{(m)},$$

where the additional subscript "0" denotes the initial state. Here, initial quantities that are not entered are zero. Next, the layers are perfectly bonded so that there are no jumps between the quantities. The resultant plate is deposited on the rigid foundation and is applied to the action of normal force at the midpoint of the upper surface. Accordingly, in the presence of a body force and a charge, the nonlinear governing equations of motion are

$$\sigma_{ij,j}^{(m)} + \left(\sigma_{kj}^{(m),0} u_{i,j}^{(m)} \right)_{,k} = \rho^{(m)} u_{i,tt}^{(m)} \text{ and } D_{i,i}^{(m)} + \left(D_i^{(m),0} u_{i,k}^{(m)} \right)_{,k} = \chi^{(m)} \varphi_{,tt}^{(m)}, \tag{4}$$

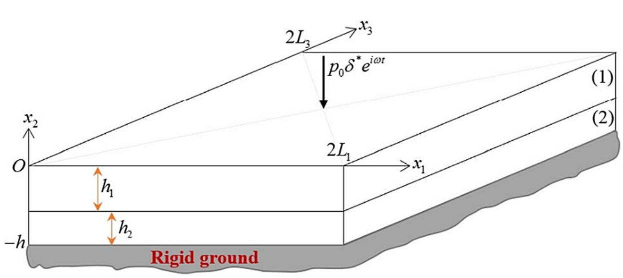

Fig. 1 Geometry of the problem

where $\rho^{(m)}$ is the mass density of mth layer, $\chi^{(m)}$ is internal charge density, t is the time parameter, and the subscript after a comma is a space derivative. In the initial state, we have

$$\sigma_{ij,j}^{(m)} + \left(\sigma_{kj}^{(m),0} u_{i,j}^{(m)}\right)_{,k} = 0 \text{ and } D_{i,i}^{(m)} + \left(D_i^{(m),0} u_{i,k}^{(m)}\right)_{,k} = 0. \tag{5}$$

Since a time-harmonic force yields compressive stress in the plate, two infinitely close states of equilibrium occur. Let $\tilde{u}_i^{(m),0}$ and $\tilde{\varphi}^{(m),0}$ be the displacement and electric potential field of the initial stress. As a result, we can write $u_i^{(m)} \cong \tilde{u}_i^{(m),0} + \alpha\tilde{u}_i^{(m)}$ and $\varphi^{(m)} \cong \varphi^{(m),0} + \alpha\varphi^{(m)}$, where $\alpha\tilde{u}_i^{(m)}$ and $\alpha\varphi^{(m)}$ are the additional displacement and the additional electric potential from the initial state to the dynamic stress state and α is dimensionless infinitely small parameter. In addition, based on this idea, stress and electric displacement components can be written in the form of $\sigma_{ij}^{(m)} = \tilde{\sigma}_{ij}^{(m),0} + \alpha\tilde{\sigma}_{ij}^{(m)}$ and $D_i^{(m)} = \tilde{D}_i^{(m),0} + \alpha\tilde{D}_i^{(m)}$. Therefore, we can write

$$\begin{aligned}
&\tilde{\sigma}_{ij,j}^{(m),0} + \alpha\tilde{\sigma}_{ij,j}^{(m)} + \tilde{\sigma}_{kj,k}^{(m),0}\tilde{u}_{i,j}^{(m),0} + \tilde{\sigma}_{kj}^{(m),0}\tilde{u}_{i,jk}^{(m),0} \\
&\quad + \alpha\tilde{\sigma}_{kj,k}^{(m),0}\tilde{u}_{i,j}^{(m)} + \alpha\tilde{\sigma}_{kj}^{(m),0}\tilde{u}_{i,jk}^{(m)} + \alpha\tilde{\sigma}_{kj,k}^{(m)}\tilde{u}_{i,j}^{(m),0} + \alpha\tilde{\sigma}_{kj}^{(m)}\tilde{u}_{i,jk}^{(m),0} \\
&\quad + \alpha^2\tilde{\sigma}_{kj,k}^{(m)}\tilde{u}_{i,j}^{(m)} + \alpha^2\tilde{\sigma}_{kj}^{(m)}\tilde{u}_{i,jk}^{(m)} = \rho^{(m)}\tilde{u}_{i,tt}^{(m),0} + \rho^{(m)}\alpha\tilde{u}_{i,tt}^{(m)}
\end{aligned} \tag{6}$$

and

$$\begin{aligned}
&\tilde{D}_{i,i}^{(m),0} + \alpha\tilde{D}_{i,i}^{(m)} + \tilde{D}_{i,k}^{(m),0}\tilde{u}_{i,k}^{(m),0} + \tilde{D}_i^{(m),0}\tilde{u}_{i,kk}^{(m),0} + \alpha\tilde{D}_{i,k}^{(m),0}\tilde{u}_{i,k}^{(m)} \\
&\quad + \alpha\tilde{D}_i^{(m),0}\tilde{u}_{i,kk}^{(m)} + \alpha\tilde{D}_{i,k}^{(m)}\tilde{u}_{i,k}^{(m),0} + \alpha\tilde{D}_i^{(m)}\tilde{u}_{i,kk}^{(m),0} + \alpha^2\tilde{D}_{i,k}^{(m)}\tilde{u}_{i,k}^{(m)} \\
&\quad + \alpha^2\tilde{D}_i^{(m)}\tilde{u}_{i,kk}^{(m)} = \chi^{(m)}\tilde{\varphi}_{,tt}^{(m),0} + \chi^{(m)}\alpha\tilde{\varphi}_{,tt}^{(m)}
\end{aligned} \tag{7}$$

According to the fundamental principles of TLTESIS [27], the amplitudes of dynamic perturbation are relatively smaller than the initial stress state's ones and there is a static and homogeneous initial stress state. In this case, the derivatives of all the initial fields are zero. Since α is infinitely small, the term including α^2 is infinitely small of second-order too. So these terms can be neglected. On the other hand, the electric problem can be treated as quasi-static. This is because we can assume that the variability of the electric field over time is relatively slow, so we can neglect the dynamic electrical state. Accordingly, the right-hand side of Eq. (7) can be neglected. Further, since dynamic force is time-harmonic, all the problem field is too. Further, since dynamic force is time-harmonic with frequency ω, all the problem field is too, and the time parameter can be discretized such as $\square^{(m)} = \hat{\square}^{(m)} e^{i\omega t}$, where e is exponential constant and i is complex unit. After the coordinate simplification rule $\hat{x}_i = x_i/h$, the coupled equations of motion are given as

$$\sigma_{ij,j}^{(m)} + \sigma_{kj}^{(m),0} u_{i,jk}^{(m)} + \rho^{(m)} h^2\omega^2 u_i^{(m)} = 0, \tag{8}$$

$$D_{i,i}^{(m)} + D_i^{(m),0} u_{i,kk}^{(m)} = 0. \tag{9}$$

Here, hats, overbars, and tildes were neglected for simplicity, as will be in the future.

The boundary-contact conditions of the problem under consideration can be summarized as follows:

$$\sigma_{21}^{(1)}\Big|_{x_2=0} = 0,\ \sigma_{32}^{(1)}\Big|_{x_2=0} = 0,\ \sigma_{22}^{(1)}\Big|_{x_2=0} = -p_o\delta^*, \tag{10}$$

$$\sigma_{i2}^{(1)}\Big|_{x_2=-h_1/h} = \sigma_{i2}^{(2)}\Big|_{x_2=-h_1/h},\ u_i^{(1)}\Big|_{x_2=-h_1/h} = u_i^{(2)}\Big|_{x_2=-h_1/h}, \tag{11}$$

$$D_2^{(1)}\Big|_{x_2=-h_1/h} = D_2^{(2)}\Big|_{x_2=-h_1/h},\ \varphi^{(1)}\Big|_{x_2=-h_1/h} = \varphi^{(2)}\Big|_{x_2=-h_1/h}, \tag{12}$$

$$\left(\sigma_{\ell j}^{(m)} + \sigma_{\ell\ell}^{(m),0} u_{j,\ell}^{(m)}\right)\Big|_{x_\ell=0,2a_\ell/h} = 0,\ \left(D_i^{(m)} + D_\ell^{(m),0} u_{\ell,i}^{(m)}\right)\Big|_{x_\ell=0,2a_\ell/h} = 0, \tag{13}$$

$$u_i^{(2)}\Big|_{x_2=-1} = 0, \text{ and } \varphi|_{x_2=0,-1} = 0, \tag{14}$$

where $\ell = 1, 3$, p_0 is the intensity of the force, and δ^* is the Dirac-delta function in the form of $\delta^* = \delta\left(\left(x_1/h - a_1/h\right)^2 + \left(x_3/h - a_3/h\right)^2\right)$. Here, Eq. (10) is mechanical traction-free conditions, Eq. (11) is mechanical complete clamped conditions, Eq. (12) is electrical complete clamped conditions, Eq. (13) is mechanically and electrically open conditions, and Eq. (14) is mechanically free and electrically open conditions. This completes the presentation of the formulation of the problem.

Solution Procedure

This section derives a three-dimensional finite element model for the current problem. Here, the first aim is to obtain the variational formulation of the problem. In this part of the paper, we shall make symbolic computations due to wide statements. The coupled equations of motion in Eqs. (8) and (9) can be organized, in a vector form, as follows:

$$\{\boldsymbol{\Sigma}\} = \left\{ \Sigma_1^{(1)}\ \Sigma_2^{(1)}\ \Sigma_3^{(1)}\ \Sigma_1^{(2)}\ \Sigma_2^{(2)}\ \Sigma_3^{(2)} \right\}^T \text{ and } \{\boldsymbol{D}\} = \left\{ \mathrm{D}^{(1)}\ \mathrm{D}^{(2)} \right\}^T, \tag{15}$$

where the upper "T" is the transpose operator. Let $\left\{\mathrm{V}_i^{(m)}\right\}$ and $\left\{\mathrm{F}^{(m)}\right\}$ be the admissible displacement and electric potential. Let us multiply Eq. (15) with the admissible displacement $\left\{\mathrm{V}_i^{(m)}\right\}$ and the admissible electric potential $\left\{\mathrm{F}^{(m)}\right\}$ and integrate the resultant equations after summing them up over volume V. So we can write

$$\int_V \left[\begin{array}{r} \{L\}^T[\sigma]^T\{\mathrm{V}\} + \left\{\sigma^0\right\}^T\left[(L \odot L) \otimes \{\mathrm{U}\}^T\right]\{\mathrm{V}\} + \rho\omega^2 h^2 \{\mathrm{U}\}^T\{\mathrm{V}\} \\ + \left\{ \{L\}^T\{\mathrm{D}\} + \left\{D^0\right\}^T\left[(L.L)^T\{\mathrm{U}\}\right]\mathrm{I} \right\}\{\mathrm{F}\} \end{array} \right] dV = 0, \tag{16}$$

where "⊙" is the Hadamard product, "⊗" is the Kronecker product, "." is the dot product, and $\mathrm{I} = \left\{ 1 \ 1 \ 1 \right\}^T$. In Eq. (16), other notations are as follows:

$$L = \left\{ \frac{\partial}{\partial x_i} \right\}_{3\times1}, \ \sigma = \left[\sigma_{ij}\right]_{3\times3}, \ \{\mathrm{V}\} = \left\{v_i\right\}_{3\times1}, \ \sigma^0 = \left\{\sigma^0_{ii}\right\}_{3\times1}, \ \{\mathrm{U}\} = \left\{u_i\right\}_{3\times1},$$
$$\{\mathrm{D}\} = \left\{D_i\right\}_{3\times1}, \ D^0 = \left\{D^0_i\right\}_{3\times1}, \text{ and } \{\mathrm{F}\} = \{\psi\}_{1\times1}.$$

where η_1 and η_3 are initial stress parameters; κ_1 and κ_3 are electrical initial stress parameters; and Ω is dimensionless frequency parameter.

The volume of the piezoelectric plate is discretized using n_p rectangular prisms including M nodes. For the current problem, there are four degrees of freedom over a typical master prism; namely, three displacements and one electric potential.

According to the general scheme of calculus of variation, if the derivative is transferred to the admissible terms by considering the boundary-contact conditions, we get

$$-\int_\Gamma \{\mathrm{G}\}^T\{\mathrm{V}\}dx_1dx_3 + \rho\omega^2h^2\int_V \{\mathrm{U}\}^T\{\mathrm{V}\}dV$$
$$-\int_V \left[\begin{array}{l} [\sigma]\left(\{L\}^T \otimes \{\mathrm{V}\}\right) + \left\{\sigma^0\right\}\left\{\left[\{L\}^T \otimes \{\mathrm{U}\}\right] \odot \left[\{L\}^T \otimes \{\mathrm{V}\}\right]\right\}\mathrm{I} \\ +\{\mathrm{D}\}\{L\}^T\{\mathrm{F}\} - \left\{D^0\right\}^T\left[\left(\{L\}^T \otimes \{\mathrm{U}\}\right) \odot \left(\{L\}^T \otimes \{\mathrm{F}\}\right)\right]\mathrm{I} \end{array} \right] dV = 0$$

where $\{\mathrm{G}\} = \left\{ 0 \ p_o\delta^* \ 0 \right\}^T$. As a result, we constructed the following quaternary linear form:

$$B(\mathbf{v}, \mathbf{u}, \boldsymbol{\varphi}, \boldsymbol{\psi}) = l(\mathbf{v}). \tag{17}$$

With the aid of the fundamental lemma of calculus of variation, the quaternary linear form yields the following total energy functional:

In this case, the approximated displacement and electrical potential vectors at the ith node of the master element are

$$\boldsymbol{u}^e = \left[u^e_{1i} \ u^e_{2i} \ u^e_{3i} \right]^T \text{ and } \boldsymbol{\varphi}^e = \left[\varphi^e_i\right],$$

where the letter "e" represents the related component of the master element. So the approximated displacement and electrical potential vectors, which are denoted by $\overline{\boldsymbol{u}}$ and $\overline{\boldsymbol{\varphi}}$, at an arbitrary point in the sub-volumes $V^e \subset V$ are stated as

$$-\frac{1}{2}\int_V \left[\begin{array}{c} \tilde{c}_1\left(u_{1,1}\right)^2 + \tilde{c}_3\left(u_{2,2}\right)^2 + \tilde{c}_1\left(u_{3,3}\right)^2 + \left(u_{1,2} + u_{2,1}\right)^2 + \left(u_{2,3} + u_{3,2}\right)^2 + \tilde{c}_5\left(u_{1,3} + u_{3,1}\right)^2 \\ +2\tilde{c}_2\left\{u_{1,1}u_{2,2} + u_{2,2}u_{3,3}\right\} + 2\tilde{c}_4 u_{1,1}u_{3,3} + \eta_1\left\{\left(u_{1,1}\right)^2 + \left(u_{2,1}\right)^2 + \left(u_{3,1}\right)^2\right\} \\ +\eta_3\left\{\left(u_{1,3}\right)^2 + \left(u_{2,3}\right)^2 + \left(u_{3,3}\right)^2\right\} - \Omega^2\left\{\left(u_1\right)^2 + \left(u_2\right)^2 + \left(u_3\right)^2\right\} \\ +2\left\{\tilde{e}_5\left(u_{1,2} + u_{2,1}\right) + \kappa_1 u_{1,1} + \kappa_3 u_{3,1}\right\}\varphi_{,1} + 2\left(\tilde{e}_1 u_{1,1} + \tilde{e}_3 u_{2,2} + \tilde{e}_1 u_{3,3} + \kappa_1 u_{1,2} + \kappa_3 u_{3,2}\right)\varphi_{,2} \\ +2\left\{\tilde{e}_5\left(u_{2,3} + u_{3,2}\right) + \kappa_1 u_{1,3} + \kappa_3 u_{3,3}\right\}\varphi_{,3} - \tilde{\gamma}_1\left(\varphi_{,1}\right)^2 - \tilde{\gamma}_3\left(\varphi_{,2}\right)^2 - \tilde{\gamma}_1\left(\varphi_{,3}\right)^2 \end{array} \right] dV - \int_\Gamma \frac{p_o}{c_{44}}\delta^* u_2 d\Gamma_2 = 0 \tag{18}$$

In Eq. (18), the following notations are used:

$$\tilde{c}_1 = \frac{c_{11}}{c_{44}}, \tilde{c}_2 = \frac{c_{13}}{c_{44}}, \tilde{c}_3 = \frac{c_{33}}{c_{44}}, \ \tilde{c}_4 = \frac{c_{12}}{c_{44}}, \tilde{c}_5 = \frac{c_{66}}{c_{44}}, \eta_1 = \frac{q_{11}}{c_{44}}, \eta_3 = \frac{q_{33}}{c_{44}}, \ \Omega = \omega h\sqrt{\frac{\rho}{c_{44}}},$$
$$\tilde{e}_1 = \frac{e_{31}}{c_{44}}, \tilde{e}_3 = \frac{e_{33}}{c_{44}}, \tilde{e}_5 = \frac{e_{15}}{c_{44}}, \tilde{\gamma}_1 = \frac{\gamma_{11}}{c_{44}}, \tilde{\gamma}_3 = \frac{\gamma_{33}}{c_{44}}, \kappa_1 = \frac{D^0_1}{2c_{44}}, \text{ and } \kappa_3 = \frac{D^0_3}{2c_{44}}, \tag{19}$$

$$\overline{\boldsymbol{u}}^e = \sum_{j=1}^{M} N_{uj} u_j^e = \boldsymbol{N}_u \boldsymbol{u}^e \text{ and } \overline{\boldsymbol{\varphi}}^e = \sum_{j=1}^{M} N_{\varphi j} \varphi_j^e = \boldsymbol{N}_\varphi \boldsymbol{\varphi}^e, \quad (20)$$

where N_{uj}^e and $N_{\varphi j}^e$ are Lagrange interpolation functions; $\boldsymbol{u}^e$ and $\boldsymbol{\varphi}^e$ are displacement and electrical potential vectors. In Eq. (20), the following notations are used:

$$\boldsymbol{u}^e = \left[u_{u11}^e \ \dots \ u_{u1M}^e \ u_{u21}^e \ \dots \ u_{u2M}^e \ u_{u31}^e \ \dots \ u_{u3M}^e \right]^T, \ \boldsymbol{\varphi}^e = \left[\varphi_1^e \ \varphi_2^e \ \dots \ \varphi_M^e \right]^T,$$

$$\boldsymbol{N}_u = \begin{bmatrix} N_1 & 0 & 0 & N_2 & 0 & 0 & \dots & N_M & 0 & 0 \\ 0 & N_1 & 0 & 0 & N_2 & 0 & 0 & \dots & N_M & 0 \\ 0 & 0 & N_1 & 0 & 0 & N_2 & 0 & 0 & \dots & N_M \end{bmatrix}, \text{ and } \boldsymbol{N}_\varphi = \left[N_1 \ N_2 \ \dots \ N_M \right].$$

It should be noted that all the computations over a master element depend on many variables. Thus, we can eliminate the problem of calculating separately for each element by transporting the master finite element to unit volume $[-1,1]\times[-1,1]\times[-1,1]$. To aim this, the transformation rule from the spatial coordinates $(\hat{x}_1, \hat{x}_2, \hat{x}_3)$ to the natural coordinates (r, s, t) can be achieved as shown below:

$$\left\{ \frac{\partial}{\partial x_1} \ \frac{\partial}{\partial x_2} \ \frac{\partial}{\partial x_3} \right\}^T = |\boldsymbol{J}|^{-1} \left\{ \frac{\partial}{\partial r} \ \frac{\partial}{\partial s} \ \frac{\partial}{\partial t} \right\}^T, \quad (21)$$

where $|\boldsymbol{J}|$ is the Jacobian factor defined by

$$\boldsymbol{J} = \begin{bmatrix} \frac{\partial x_1}{\partial r} & \frac{\partial x_2}{\partial r} & \frac{\partial x_3}{\partial r} \\ \frac{\partial x_1}{\partial s} & \frac{\partial x_2}{\partial s} & \frac{\partial x_3}{\partial s} \\ \frac{\partial x_1}{\partial t} & \frac{\partial x_2}{\partial t} & \frac{\partial x_3}{\partial t} \end{bmatrix}.$$

Here, we prefer eight-noded isoparametric brick volume to use. The interpolation functions used herein can be listed as follows Petyt [38]:

$$N_1 = \frac{1}{8}(1-r)(1-s)(1+t), \ N_2 = \frac{1}{8}(1+r)(1-s)(1+t), \ N_3 = \frac{1}{8}(1+r)(1+s)(1+t),$$
$$N_4 = \frac{1}{8}(1-r)(1+s)(1+t), \ N_5 = \frac{1}{8}(1-r)(1-s)(1-t), \ N_6 = \frac{1}{8}(1+r)(1-s)(1-t),$$
$$N_7 = \frac{1}{8}(1+r)(1+s)(1-t), \text{ and } N_8 = \frac{1}{8}(1-r)(1+s)(1-t),$$

with the Jacobian factor $|\boldsymbol{J}| = \alpha\beta\gamma$. Here, α, β, and γ are the lengths of the master finite element.

According to the Gauss-Ostrogradsky theorem, if grouping by computing the derivative with respect to the displacements and electric potential coefficients after substituting Eq. (20) with the Jacobian transformation (21) into the total energy functional in Eq. (18), we obtain the following set of local equations:

$$\left(\boldsymbol{K}_{uu}^e - \Omega^2 \boldsymbol{M}_{uu}^e\right)\boldsymbol{u}^e + \boldsymbol{K}_{u\varphi}^e \boldsymbol{\varphi}^e = \boldsymbol{f}_u^e \quad (22)$$

$$\boldsymbol{K}_{\varphi u}^e \boldsymbol{u}^e + \boldsymbol{K}_{\varphi\varphi}^e \boldsymbol{\varphi}^e = 0 \quad (23)$$

$$\boldsymbol{K}_{uu}^e = \begin{bmatrix} \boldsymbol{K}_{11}^{uu} & \boldsymbol{K}_{12}^{uu} & \boldsymbol{K}_{13}^{uu} \\ & \boldsymbol{K}_{22}^{uu} & \boldsymbol{K}_{23}^{uu} \\ sym. & & \boldsymbol{K}_{33}^{uu} \end{bmatrix},$$

$$\boldsymbol{M}_{uu}^e = \begin{bmatrix} \boldsymbol{M}_{11}^{uu} & \boldsymbol{M}_{12}^{uu} & \boldsymbol{M}_{13}^{uu} \\ & \boldsymbol{M}_{22}^{uu} & \boldsymbol{M}_{23}^{uu} \\ sym. & & \boldsymbol{M}_{33}^{uu} \end{bmatrix},$$

$$\boldsymbol{K}_{u\varphi}^e = \begin{Bmatrix} \boldsymbol{K}_1^{u\varphi} \\ \boldsymbol{K}_2^{u\varphi} \\ \boldsymbol{K}_3^{u\varphi} \end{Bmatrix}, \ \boldsymbol{f}_u^e = \begin{Bmatrix} \boldsymbol{f}_1^u \\ \boldsymbol{f}_2^u \\ \boldsymbol{f}_3^u \end{Bmatrix},$$

$$\boldsymbol{\varphi}^e = \left[\boldsymbol{\varphi}^e\right], \ \boldsymbol{K}_{\varphi u}^e = \left[\boldsymbol{K}_{u\varphi}^e\right]^T, \text{ and } \boldsymbol{K}_{\varphi\varphi}^e = \left[\boldsymbol{K}^{\varphi\varphi}\right],$$

where $\boldsymbol{K}_{uu}^e$ is the local stiffness matrix, $\boldsymbol{M}_{uu}^e$ is the local mass matrix, $\boldsymbol{K}_{u\varphi}^e$ is the local coupled electro-elastic matrix, $\boldsymbol{K}_{\varphi\varphi}^e$ is the local electric matrix, and $\boldsymbol{f}_u^e$ is the local force vector. According to the general scheme of our method, the explicit forms of the matrices and vectors are given as follows:

$$\boldsymbol{K}_{11}^{uu} = \int_{-1}^{1}\int_{-1}^{1}\int_{-1}^{1} \left[\left(\tilde{c}_1 + \eta_1\right) \frac{\beta\gamma}{\alpha} \frac{\partial N_i}{\partial r}\frac{\partial N_j}{\partial r} + \frac{\alpha\gamma}{\beta}\frac{\partial N_i}{\partial s}\frac{\partial N_j}{\partial s} + \left(\tilde{c}_5 + \eta_3\right)\frac{\beta\alpha}{\gamma}\frac{\partial N_i}{\partial t}\frac{\partial N_j}{\partial t} \right] drdsdt$$

$$K_{12}^{uu}=\int_{-1}^{1}\int_{-1}^{1}\int_{-1}^{1}\left[\frac{\partial N_i}{\partial r}\frac{\partial N_j}{\partial s}+\tilde{c}_2\frac{\partial N_i}{\partial s}\frac{\partial N_j}{\partial r}\right]\gamma drdsdt$$

$$K_{13}^{uu}=\int_{-1}^{1}\int_{-1}^{1}\int_{-1}^{1}\left[\tilde{c}_5\frac{\partial N_i}{\partial r}\frac{\partial N_j}{\partial t}+\tilde{c}_4\frac{\partial N_i}{\partial t}\frac{\partial N_j}{\partial r}\right]\beta drdsdt$$

$$K_{22}^{uu}=\int_{-1}^{1}\int_{-1}^{1}\int_{-1}^{1}\left[\left(\eta_1+1\right)\frac{\beta\gamma}{\alpha}\frac{\partial N_i}{\partial r}\frac{\partial N_j}{\partial r}+\tilde{c}_3\frac{\alpha\gamma}{\beta}\frac{\partial N_i}{\partial s}\frac{\partial N_j}{\partial s}+\left(\eta_3+1\right)\frac{\beta\alpha}{\gamma}\frac{\partial N_i}{\partial t}\frac{\partial N_j}{\partial t}\right]drdsdt$$

$$K_{23}^{uu}=\int_{-1}^{1}\int_{-1}^{1}\int_{-1}^{1}\left[\frac{\partial N_i}{\partial s}\frac{\partial N_j}{\partial t}+\tilde{c}_2\frac{\partial N_i}{\partial t}\frac{\partial N_j}{\partial s}\right]\alpha drdsdt$$

$$K_{33}^{uu}=\int_{-1}^{1}\int_{-1}^{1}\int_{-1}^{1}\left[\left(\tilde{c}_5+\eta_1\right)\frac{\beta\gamma}{\alpha}\frac{\partial N_i}{\partial r}\frac{\partial N_j}{\partial r}+\frac{\alpha\gamma}{\beta}\frac{\partial N_i}{\partial s}\frac{\partial N_j}{\partial s}+\left(\tilde{c}_1+\eta_3\right)\frac{\alpha\beta}{\gamma}\frac{\partial N_i}{\partial t}\frac{\partial N_j}{\partial t}\right]drdsdt$$

$$M_{11}^{uu}=\int_{-1}^{1}\int_{-1}^{1}\int_{-1}^{1}\alpha\beta\gamma N_iN_jdrdsdt$$

$$M_{22}^{uu}=\int_{-1}^{1}\int_{-1}^{1}\int_{-1}^{1}\alpha\beta\gamma N_iN_jdrdsdt$$

$$M_{33}^{uu}=\int_{-1}^{1}\int_{-1}^{1}\int_{-1}^{1}\alpha\beta\gamma N_iN_jdrdsdt$$

$$K_1^{ue}=\int_{-1}^{1}\int_{-1}^{1}\int_{-1}^{1}\left[\kappa_1\left(\frac{\beta\gamma}{\alpha}\frac{\partial N_i}{\partial r}\frac{\partial N_j}{\partial r}+\frac{\alpha\gamma}{\beta}\frac{\partial N_i}{\partial s}\frac{\partial N_j}{\partial s}+\frac{\beta\alpha}{\gamma}\frac{\partial N_i}{\partial t}\frac{\partial N_j}{\partial t}\right)+\tilde{e}_5\gamma\frac{\partial N_i}{\partial r}\frac{\partial N_j}{\partial s}+\tilde{e}_1\gamma\frac{\partial N_i}{\partial s}\frac{\partial N_j}{\partial r}\right]drdsdt$$

$$K_2^{ue}=\int_{-1}^{1}\int_{-1}^{1}\int_{-1}^{1}\left[\tilde{e}_5\frac{\beta\gamma}{\alpha}\frac{\partial N_i}{\partial r}\frac{\partial N_j}{\partial r}+\tilde{e}_3\frac{\alpha\gamma}{\beta}\frac{\partial N_i}{\partial s}\frac{\partial N_j}{\partial s}+\tilde{e}_5\frac{\beta\alpha}{\gamma}\frac{\partial N_i}{\partial t}\frac{\partial N_j}{\partial t}\right]drdsdt$$

$$K_3^{ue}=\int_{-1}^{1}\int_{-1}^{1}\int_{-1}^{1}\left[\kappa_3\left(\frac{\beta\gamma}{\alpha}\frac{\partial N_i}{\partial r}\frac{\partial N_j}{\partial r}+\frac{\alpha\gamma}{\beta}\frac{\partial N_i}{\partial s}\frac{\partial N_j}{\partial s}+\frac{\alpha\beta}{\gamma}\frac{\partial N_i}{\partial t}\frac{\partial N_j}{\partial t}\right)+\tilde{e}_1\alpha\frac{\partial N_i}{\partial s}\frac{\partial N_j}{\partial t}+\tilde{e}_5\alpha\frac{\partial N_i}{\partial t}\frac{\partial N_j}{\partial s}\right]drdsdt$$

$$K^{\varphi\varphi}=\int_{-1}^{1}\int_{-1}^{1}\int_{-1}^{1}\left[-\tilde{\gamma}_1\frac{\beta\gamma}{\alpha}\frac{\partial N_i}{\partial r}\frac{\partial N_j}{\partial r}-\tilde{\gamma}_3\frac{\alpha\gamma}{\beta}\frac{\partial N_i}{\partial s}\frac{\partial N_j}{\partial s}-\tilde{\gamma}_1\frac{\alpha\beta}{\gamma}\frac{\partial N_i}{\partial t}\frac{\partial N_j}{\partial t}\right]drdsdt$$

$$f_2^u=-\frac{p_o}{c_{44}}N_{hq}\Big|_{x_1=a_1/h,x_2=0,x_3=a_3/h}$$

Here, the matrices and vectors that is not entered are zero. It is seen that there is only non-zero one entry of the vector f_u^e. By assembling the set of the local element-vector equations, the global dynamic equilibrium equations can be obtained as follows:

$$\left(K_{uu}-\Omega^2M_{uu}\right)u+K_{u\varphi}\varphi=f_u \quad (24)$$

$$K_{\varphi u}u+K_{\varphi\varphi}\varphi=0, \quad (25)$$

where K_{uu} is the global stiffness matrix, M_{uu} is the global mass matrix, $K_{u\varphi}$ is the global coupled electro-elastic matrix, $K_{\varphi\varphi}$ is the global electric matrix, and f_u is the global force vector.

To obtain the solution to the problem, we, first, trash the corresponding rows/columns of the last globalized equations of motion by imposing the boundary-contact conditions. So, we eliminate the singularity of the globalized system. As a result, we obtain the values of the displacement and electric potential at the nodes, so that these values can be transformed to stress values using Hooke's law.

Numerical Results and Discussions

In this section, numerical results on forced vibration of the bi-layered piezoelectric plates with initial stress are given and discussed. Let us define the geometrical factors

$$\mathrm{a} = \frac{a_1}{a_3},\ h_P = \frac{h}{2a_1},\ \text{and}\ h_L = \frac{h_1}{h_2}, \tag{26}$$

where a is the aspect ratio, h_P is the plate's thickness ratio, and h_L is the layer's thickness ratio.

For the current investigation, while Lead Zirconium Titanate (PZT - 4) with $c_{44} = 25.6\,GPa$, $e_{15} = 12.7\,C/m^2$, and $\gamma_{11} = 7.625\,nF/m$, is chosen for the upper layer, Barium Titanate ($BaTiO_3$) with $c_{44} = 44\,GPa$, $e_{15} = 11.4\,C/m^2$, and $\gamma_{11} = 1.115\,nF/m$ is used for the bottom layer [39]. In particular, we consider the case where $\mathrm{a} = 1$, $h_P = 0.2$, $h_L = 1$, $\Omega = \Omega^{(1)} = \Omega^{(2)}$, $\eta = \eta_1^{(m)} = \eta_3^{(m)}$, $\Omega = 0$, and $\eta = 0$ unless otherwise specified.

Numerical Model Validation

Herein, the numerical model is validated by doing relative error analysis and comparing our results with available literature.

According to the general principles of the finite element method, when the mesh number increases, the numerical results must become better. Because improving the number yields a smaller mesh size and the data is better interpolated across the physical domains. This motivates us to present an error analysis for our algorithm. In this scope, let us consider the following norm functions:

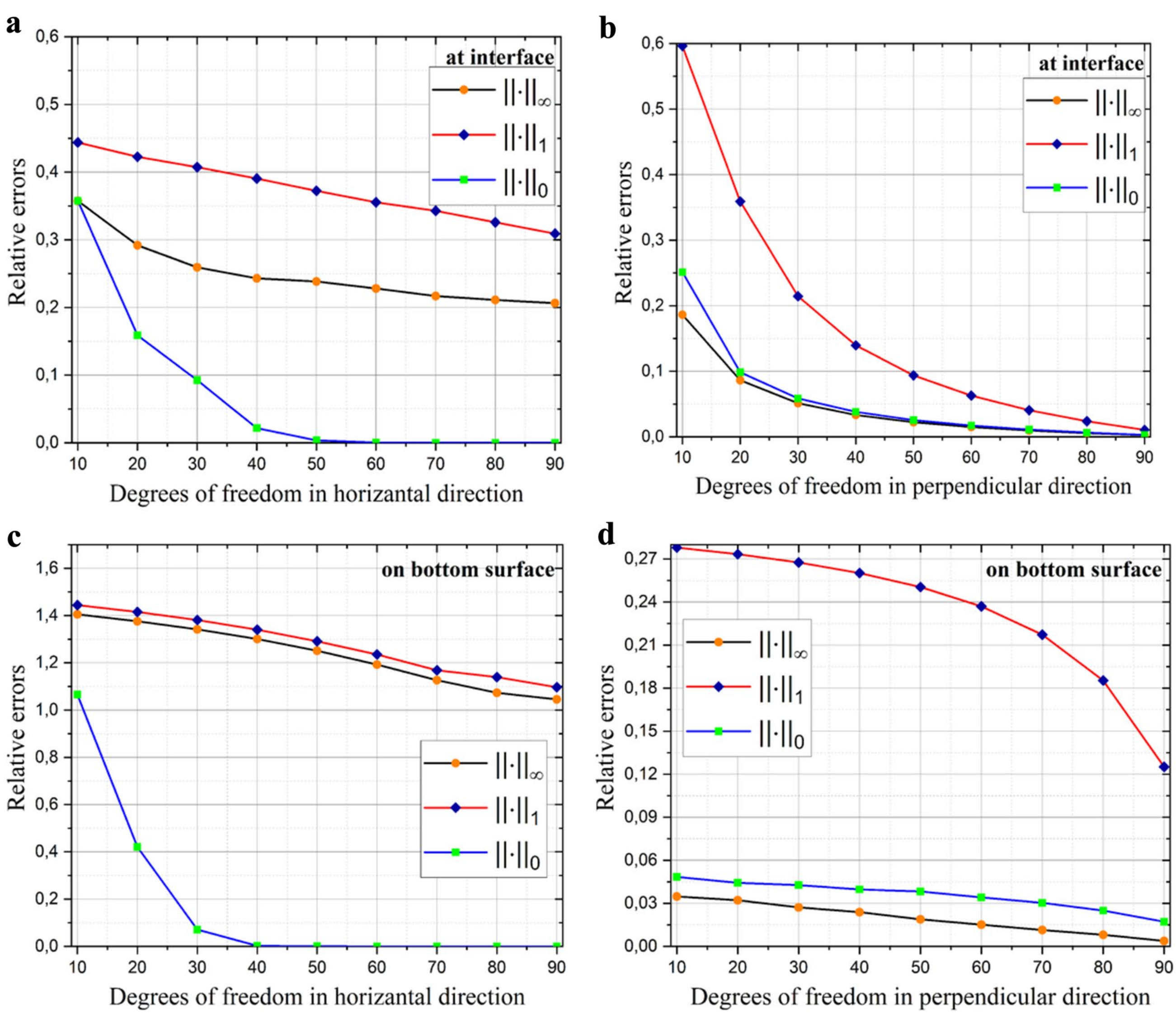

Fig. 2 Convergence rates in error norms for the number of meshes in the directions of horizontal and vertical axes at interface (**a**, **b**) and on bottom surface (**c**, **d**.)

$$\|x\|_\infty = \max_i \|x_i\|_\infty,\ \|x\|_1 = \sum_i \|x_i\|_1,\ \text{and}\ \|x\|_0 = \sqrt{\sum_i \|x_i\|_0^2},$$

which are the maximum norm, L_1-norm, and the Euclidean norm, respectively. Figure 2 sheds light on how the relative error functions behave for increasing mesh numbers both in perpendicular and horizontal directions at the interface (Fig. 2a, b) and on the bottom surface (Fig. 2c, d). The distributions of the graphs prove that the values of the relative error converge to zero as the mesh number increases. This means that the calculations for a reasonable number of finite elements have high accuracy. By the way, the converge has a quadratic character. It should be noted that these graphs were plotted by varying the mesh number in one direction while the one in the other direction was kept fixed.

Above, a convergence analysis was submitted via certain error norms. But, the results from our algorithm must be supported well with ones in the available literature. First, our problem turns into an elastic medium one for the following case:

$$c_{11}^{(m)} = c_{33}^{(m)} = \lambda^{(m)} + 2\mu^{(m)},\ c_{12}^{(m)} = c_{13}^{(m)} = \lambda^{(m)},$$
$$c_{44}^{(m)} = c_{66}^{(m)} = \mu^{(m)},\ e_{ij}^{(m)} = \gamma_{ij}^{(m)} = 0.$$

But, while doing this reduction, we must trash rows and columns of the system related to electrical parts in Eqs. (24) and (25). Otherwise, the PC algorithm does not run due to singularity. Further, some geometrical configurations can also be obtained by changing certain parameters. Based on these ideas, we can check the validity of the numerical results.

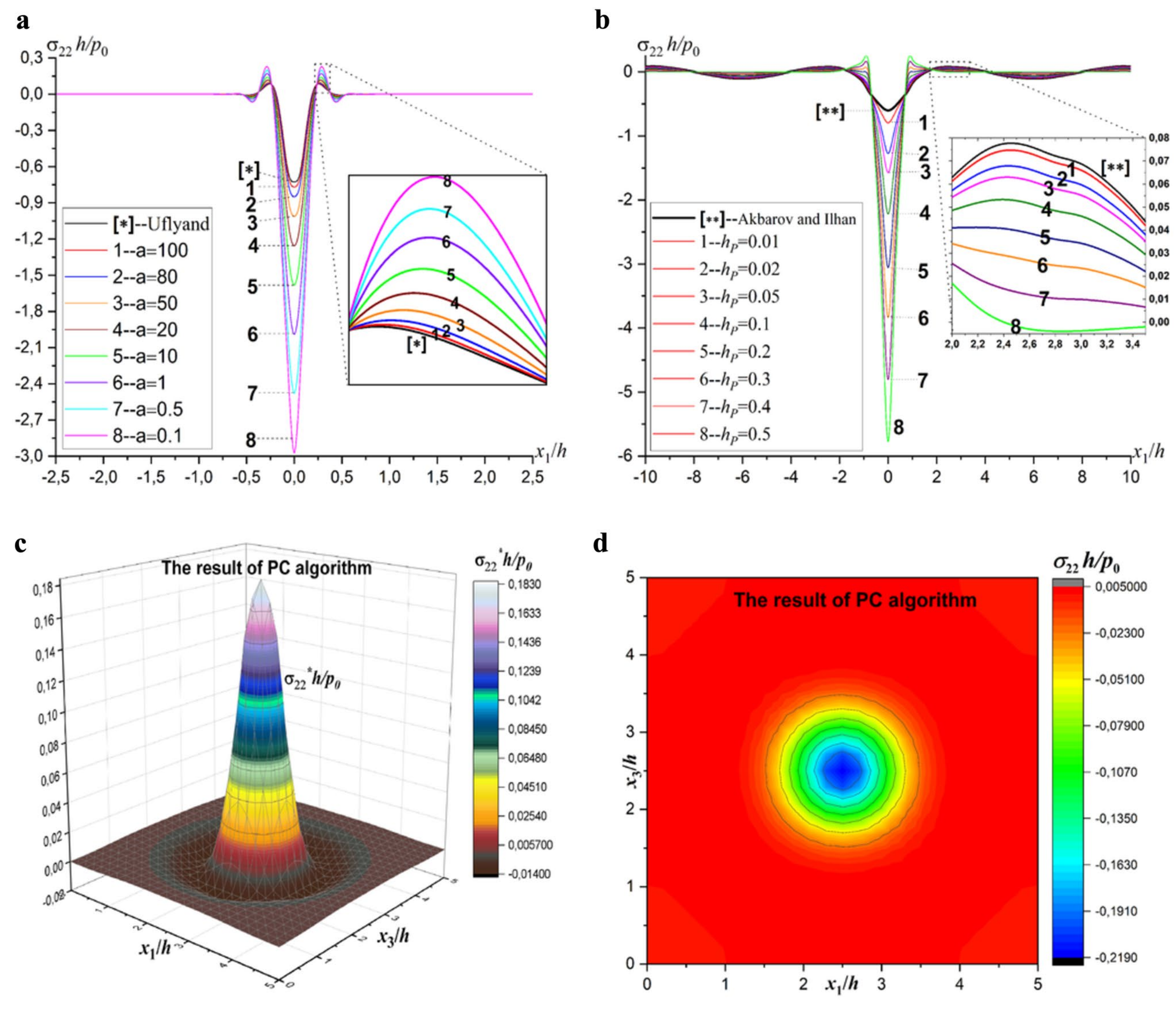

Fig. 3 Comparison of our results with the ones of **a** Uflyand [40], **b** Akbarov and Ilhan [41], **c** Daşdemir and Eröz [42], and **d** Daşdemir [43]

Let us consider four different cases for comparison analysis now. For the case where a $\to \infty$, i.e. $a_1 \to \infty$ and $a_3 \to 0$ in an elastic medium, the skeleton of the bi-layered plate takes shape the one considered by Uflyand [40] for $\nu = 0.33$ (Case I), where ν is Poisson ratio. Clearly, while one length of the plate grows up, the other is selected as small as possible. As $h_L \to \infty$, i.e., $h_P \to 0$, for a fixed height of the upper layer, the geometry of our piezoelectric problem becomes similar to Lamb's problem in the paper of Akbarov and Ilhan [41] (Case II). For both cases, our numerical results must approach the ones in the mentioned studies.

Selecting the same material in each layer for an elastic (non-electrical) medium, our problem turns exactly into the one that was considered by Daşdemir and Eröz [42] (Case III). Further, selecting the same piezoelectric material for each layer leads to obtaining a particular case that was considered by Daşdemir [39] (Case IV). For the last two cases, our graphs must coincide perfectly with the related ones under the same assumptions.

Figure 3a, b show that the numerical results (starred and double-starred graphs) under Case I and Case II converge to the one of Uflyand [40] and Akabrov and Ilhan [41, Fig. 3a, P-P, $\Omega = 1$]. Besides, Fig. 3c, d also prove that our graphs are exactly the same with the ones of Daşdemir and Eröz [42, pp. 336, Fig. 3a] and Daşdemir [43, pp. 76, Fig. 2a]. Note that $\sigma^*_{22}h/p_0 = -\sigma_{22}h/p_0$ and the graphs in Fig. 3c, d were plotted by using our PC algorithm. These inferences validate the above prediction, confirming the validity of our results.

In addition to the above, it is clear that as $h_P \to 0$ and $\Omega \to 0$, the problem under consideration is the well-known Boussinesq problem, which was considered by Timoshenko and Godier [44, p. 85], and thereby, the numerical results must imply the analytical solution of the mentioned author. Besides, according to Robin type boundary condition in Eq. (13) must converge to zero as $\eta \to 0$. These are indeed the cases in Fig. 3. Consequently, the validity and reliability of the PC algorithm are proven by the agreement of the numerical results well with the foregoing mechanical considerations.

Evaluation of Results

Herein, to get more insight into various aspects of the problem and to highlight the influence of certain system parameters on the dynamic behavior of the bi-layered piezoelectric plates, a numerical evaluation of the solution is conducted for a wide variety of cases.

First, let us investigate three-dimensional graphs of the normal stress $\sigma_{22}h/p_0$ on the plane $x_2/h = -1$ for various values of geometric and problem parameters. This allows us to understand the dynamic behavior of the plate. Figure 4 provides three-dimensional distributions of $\sigma_{22}h/p_0$ for the case where $h_L = 4$ (Fig. 4a), $h_L = 2$ (Fig. 4b), $h_L = 1$ (Fig. 4c), $h_L = 0.5$ (Fig. 4d), $h_L = 0.25$ (Fig. 4e), and $h_L = 0.2$ (Fig. 4f). While Fig. 5 shows the variations of $\sigma_{22}h/p_0$ for $h_P = 0.05$ (Fig. 5a), $h_P = 0.1$ (Fig. 5b), $h_P = 0.2$ (Fig. 5c), $h_P = 0.3$ (Fig. 5d), $h_P = 0.4$ (Fig. 5e), and $h_P = 0.5$ (Fig. 5f), Fig. 6 indicates how to effect the mentioned behavior for a = 10 (Fig. 6a), a = 5 (Fig. 6b), a = 2 (Fig. 6c), a = 0.5 (Fig. 6d), a = 0.2 (Fig. 6e), and a = 0.1 (Fig. 6f). Further, Fig. 7 displays the three-dimensional oscillations of $\sigma_{22}h/p_0$ for $\eta = -0.06$ (Fig. 6a), $\eta = -0.04$ (Fig. 6b), $\eta = -0.02$ (Fig. 6c), $\eta = 0.02$ (Fig. 6d), $\eta = 0.04$ (Fig. 6e), and $\eta = 0.06$ (Fig. 6f).

The graphs indicate that the stress distributions occur in five main circular regions, i.e., central (brown colored), moderate (red colored), minor (yellow colored), transition (blue colored), and free (purple colored) regions. The first three of these are very important. The greatest effect of the dynamic force on the piezoelectric plate intensifies over the central (brown-colored) region near the point $P = (2.5, 2.5)$. To be clear, the central, moderate, and minor regions can be represented geometrically as $\left(x_1/h - 2.5\right)^2 + \left(x_2/h - 2.5\right)^2 < r_1^2$, $r_1^2 < \left(x_1/h - 2.5\right)^2 + \left(x_2/h - 2.5\right)^2 < r_2^2$, and $r_2^2 < \left(x_1/h - 2.5\right)^2 + \left(x_2/h - 2.5\right)^2 < r_3^2$, respectively. The values of r_1, r_2, and r_3 can be detected from the graphs and are almost constant (despite quite small changes). In other regions, the stress $\sigma_{22}h/p_0$ damps almost. According to the graphs of Figs. 4, 5, 6 and 7, while the ratio h_L and the parameter η have an indirect relation on the distributions of the stress $\sigma_{22}h/p_0$, the ratios a and h_P have a direct link on the behavior of the plate.

It is concluded from Fig. 4 that, as h_L decreases, the stress $\sigma_{22}h/p_0$ increases and the central region grows up despite its limited effect. This means that PZT - 4 has a greater capability of stress isolation than $BaTiO_3$. From this, we can say that the constituent particles of $BaTiO_3$ are closer to each other than PZT - 4 and thus its medium allows strain energy transfer easier from one particle to another, increasing total stress in medium. Further, since each layer is poled in the direction of the axis Ox_2, PZT - 4 shows a bigger reaction in response to the dynamic response of the plate than $BaTiO_3$.

According to the graphs in Fig. 5, an increase in the value of the ratio h_P leads to a decrease in the stress $\sigma_{22}h/p_0$ and damps the stress. It is clearly seen that as h_P increases, central and moderate regions vanish. This causes more stress transfer between the particles of the plate, giving rise to a decrease in the stress on the bottom surface. However, it should be reasonable since this increase will cause an increase in the material cost. The ratio h_P is a great actor in the dynamic behavior of the piezoelectric plate.

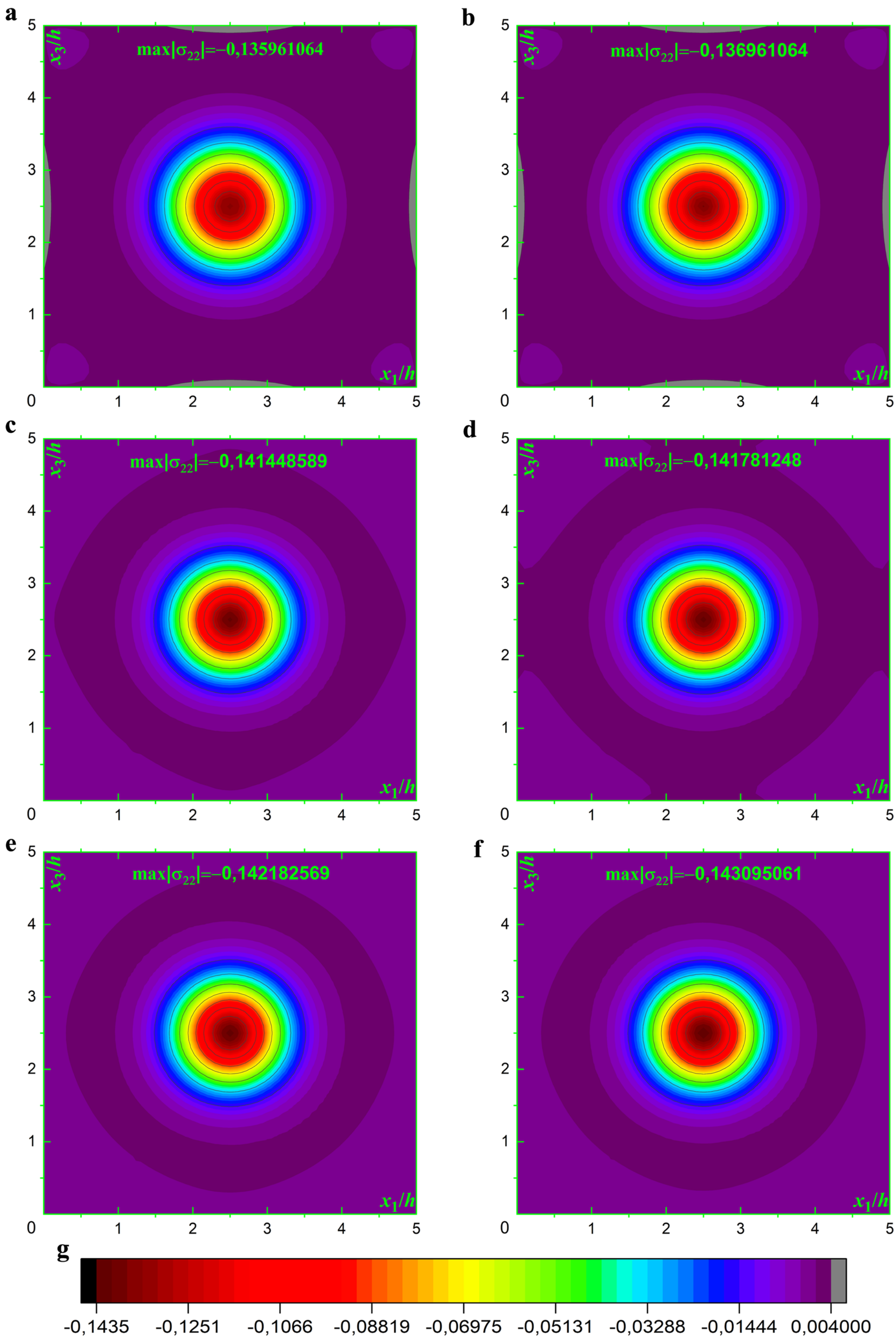

Fig. 4 Distributions of $\sigma_{22}h/p_0$ on the plane $x_2/h = -1$ under **a** $h_L = 4$, **b** $h_L = 2$, **c** $h_L = 1$, **d** $h_L = 0.5$, **e** $h_L = 0.25$, **f** $h_L = 0.2$, and **g** color scale

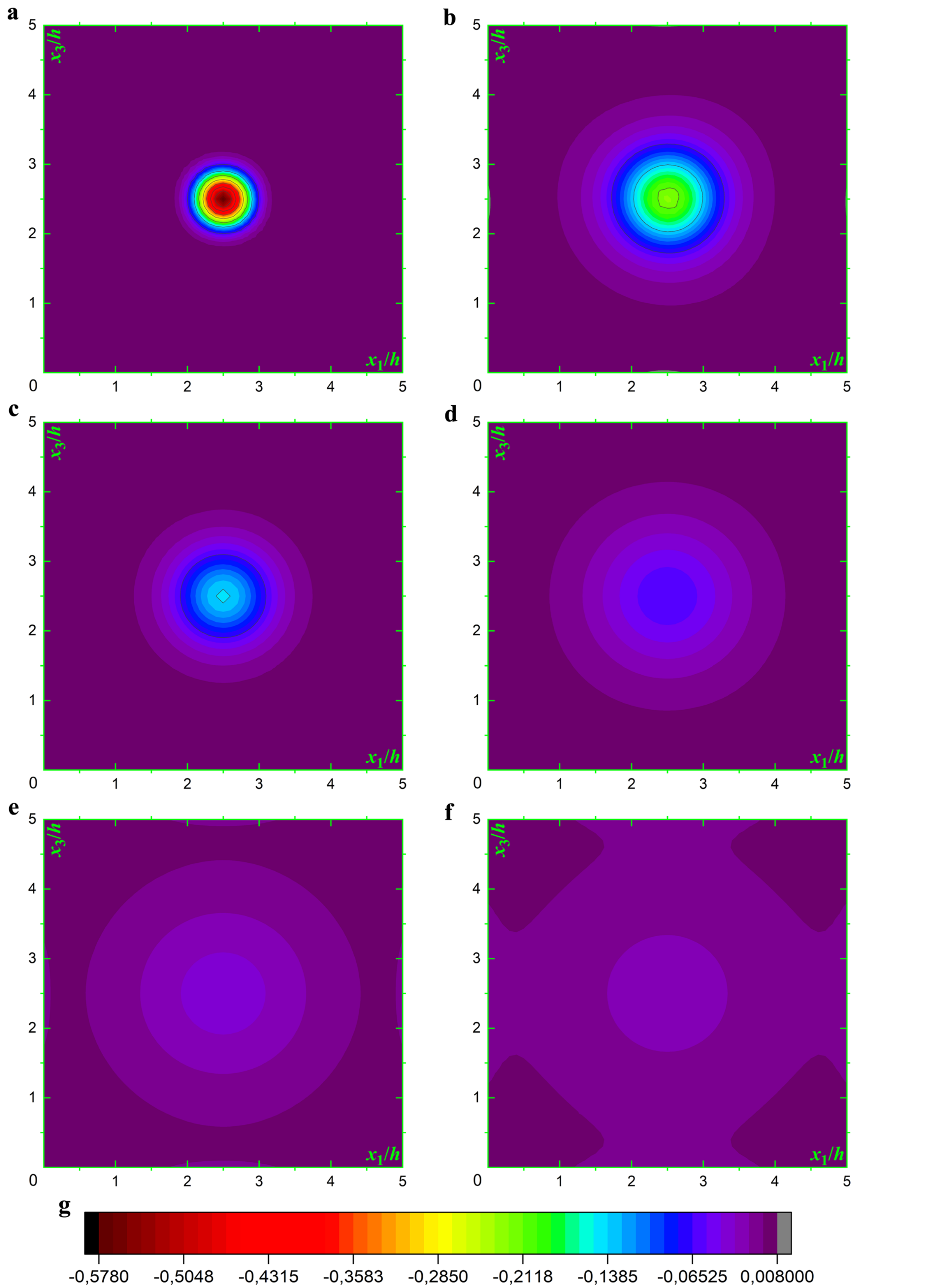

Fig. 5 Distributions of $\sigma_{22}h/p_0$ on the plane $x_2/h = -1$ under **a** $h_P = 0.05$, **b** $h_P = 0.1$, **c** $h_P = 0.2$, **d** $h_P = 0.3$, **e** $h_P = 0.4$, **f** $h_P = 0.5$, and **g** color scale

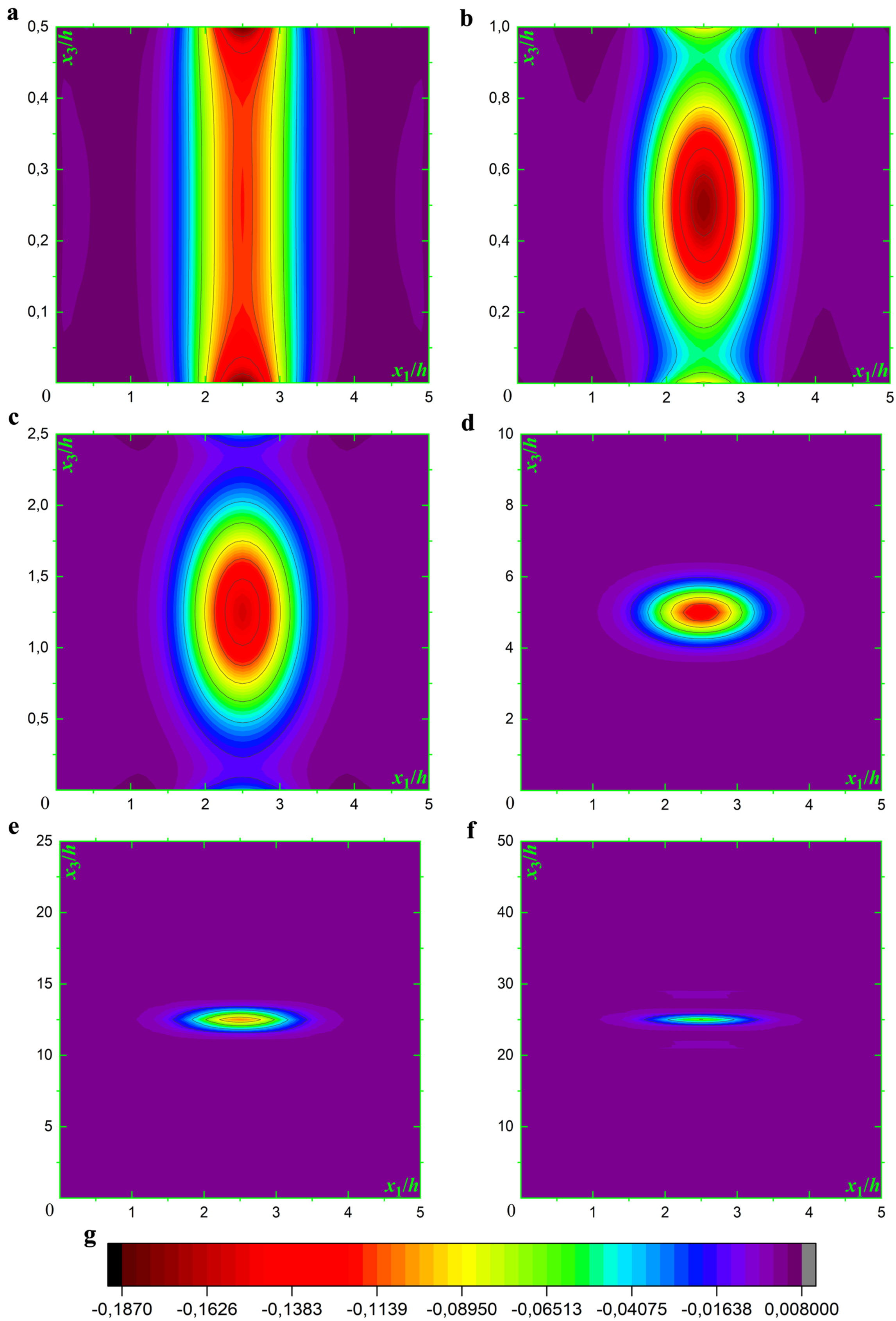

Fig. 6 Distributions of $\sigma_{22}h/p_0$ on the plane $x_2/h = -1$ under **a** a = 10, **b** a = 5, **c** a = 2, **d** a = 0.5, **e** a = 0.2, **f** a = 0.1, and **g** color scale

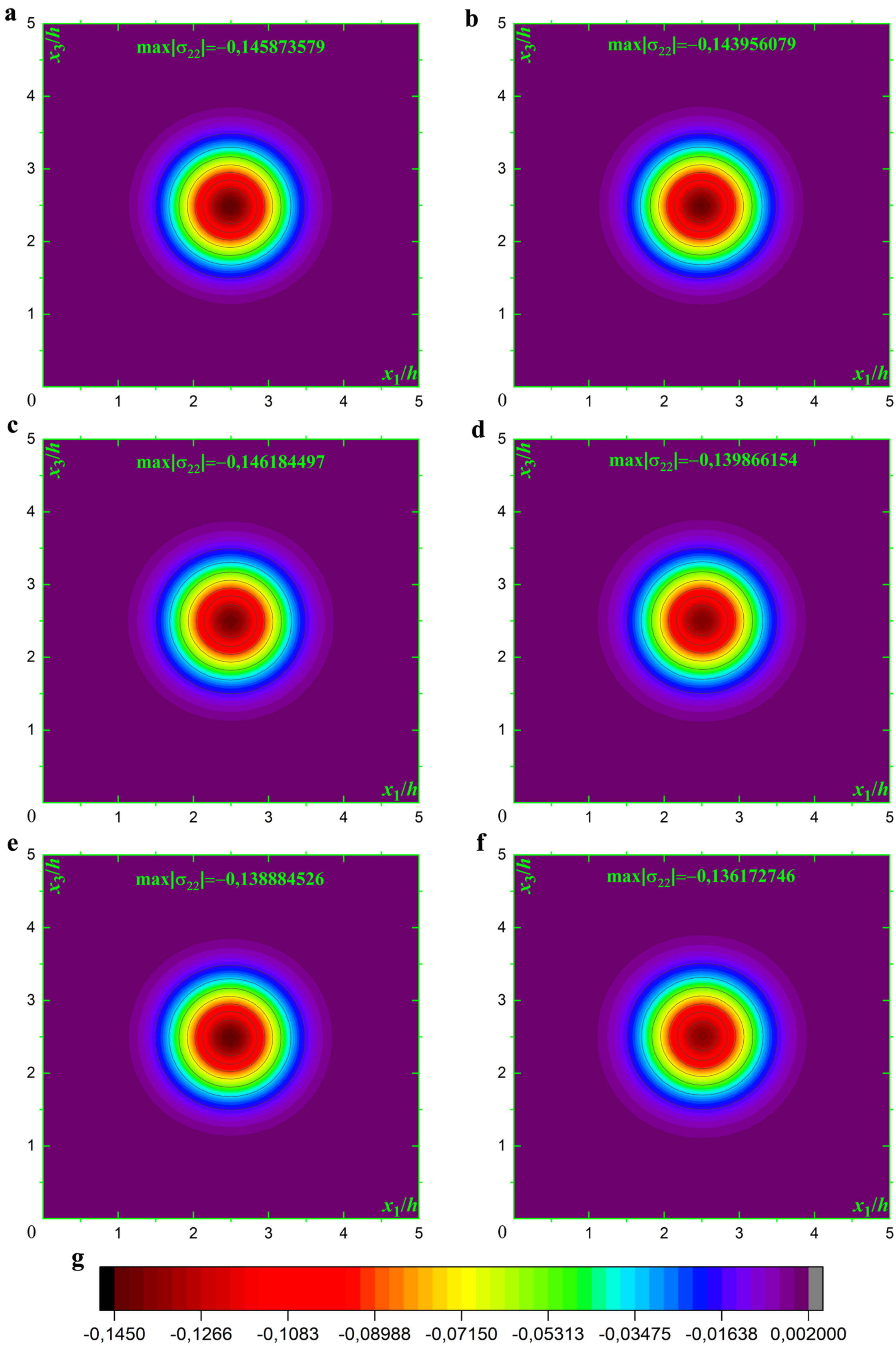

Fig. 7 Distributions of $\sigma_{22}h/p_0$ on the plane $x_2/h = -1$ under **a** $\eta = -0.06$, **b** $\eta = -0.04$, **c** $\eta = -0.02$, **d** $\eta = 0.02$, **e** $\eta = 0.04$, **f** $\eta = 0.06$, and **g** color scale

It can be observed from Fig. 6 with Fig. 4c ($h_L = 1$, a = 1) that the aspect ratio a has a considerable effect on the dynamic behavior of the plate, in both a quantitative sense and a qualitative sense. When the horizontal lengths of the plate are equal, the stress distributions take a circular shape but otherwise, they are not. To be clear, for a ≠ 1, the stress regions run along the short side. Even, from Fig. 6a, the central region occurs on both long sides. The normal stress $\sigma_{22}h/p_0$ decreases with the ratio a. For the body with greater lengths, the stress $\sigma_{22}h/p_0$ tends to spread more homogeneously. This shows that the central and moderate regions are combined by reducing them to the minor region. The graphs indicate that if ratio a is chosen less than the value of r_1, r_2, and r_3, respectively, the stress waves hit the related lateral surface of the plate and scatter along this surface. In particular, Fig. 6a shows that there exist two central regions at two lateral sides of the plate. Similarly, in Fig. 6b, two minor regions occur also. Accordingly, for the body of quite small dimensions, our investigation must be done carefully since the system can crash.

Figure 7 together with Fig. 4c ($h_L = 1$, $\eta = 0$) helps us for detecting the effect of the initial stress (compression and tensile) parameter η on the dynamic response of the piezoelectric plate. The graphs were plotted for both initial compression η^- (negative signed values) and initial tensile η^+ (positive signed values). The absolute values of the stress $\sigma_{22}h/p_0$ increase as η decreases. Accordingly, when the initial compression η^- is applied to each layer, the constituent particles of the plate become closer together, increasing the density of the medium. As a result, this facilitates the stress transfer along the particles of the plate, giving rise to increasing the total stress. Unlike this, the initial tensile η^+ further removes the particles of the plate, preventing the stress transfer as much as possible. All the graphs show that increasing initial static force diminishes the sizes of the central and moderate regions. The It is shown that the initial stress state changes dynamic behavior of the system related to resist of stress waves.

Up to now, we have investigated three-dimensional stress distributions in the bi-layered piezoelectric plate on the bottom surface for certain problem parameters. But, our main purpose is to investigate the frequency response of the plate in response to the external dynamic force at the point $(2.5, -1, 2.5)$. The next ones do this.

Figure 8 provides certain results to explain the relationships between $\sigma_{22}h/p_0$ and Ω for various values of the ratio h_L. The numerical results coincide with the ones in Fig. 4. It can be seen that the graphs have peak points for certain values of Ω. These are called resonance values and represented by $\Omega *$. For example, $\Omega * \approx 1.0$ for $h_L = 0.5$. The absolute values of the stress $\sigma_{22}h/p_0$ increase routinely with Ω before $\Omega *$, but the oscillation number of the stress waves increases after the resonance value. This means that the system is stable before this value but after it, the influence of the responsible parameter can crash the system, making unstable case up. As the ratio h_L decreases, the resonance values of the plate decrease also. One can say that increasing the layer's thickness ratio contributes significantly to the stability of the system. Further, it is concluded that the number of maximal values of the stress $\sigma_{22}h/p_0$ increases as the ratio h_L decreases. In addition to the differences in the characteristics of the resonance values, it is observed that there is a qualitative effect of their spectrum caused by the applied force. Thus, it turns out that the smaller the ratio h_L, that is, the closer the interface to the upper surface, the more irregular transition of stress waves between the particles of

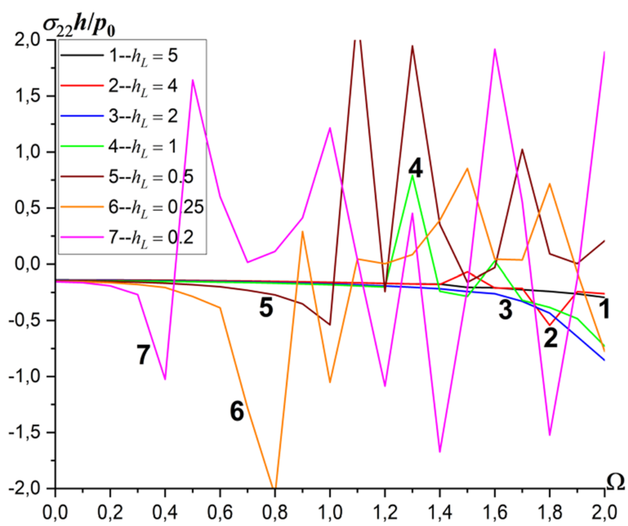

Fig. 8 Effect of the ratio h_L on the dependency between $\sigma_{22}h/p_0$ and Ω

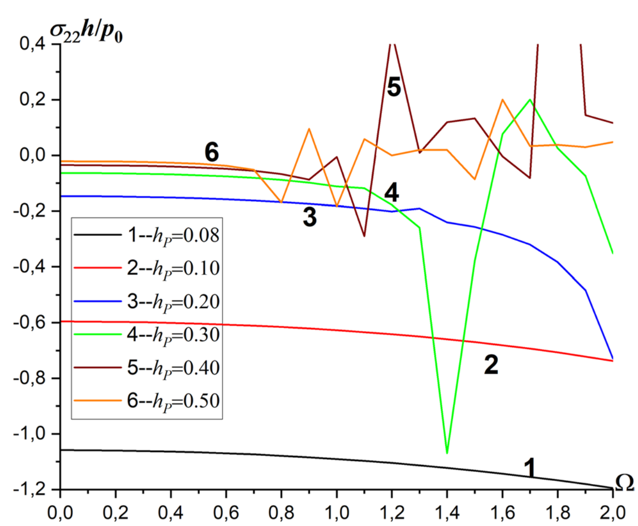

Fig. 9 Effect of the ratio h_P on the dependency between $\sigma_{22}h/p_0$ and Ω

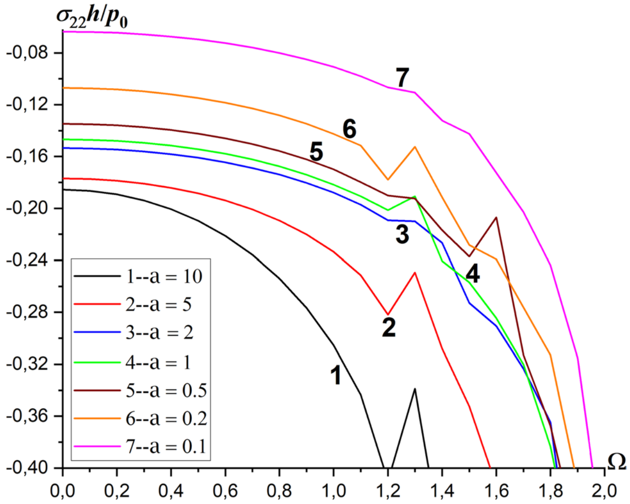

Fig. 10 Effect of the ratio a on the dependency between $\sigma_{22}h/p_0$ and Ω

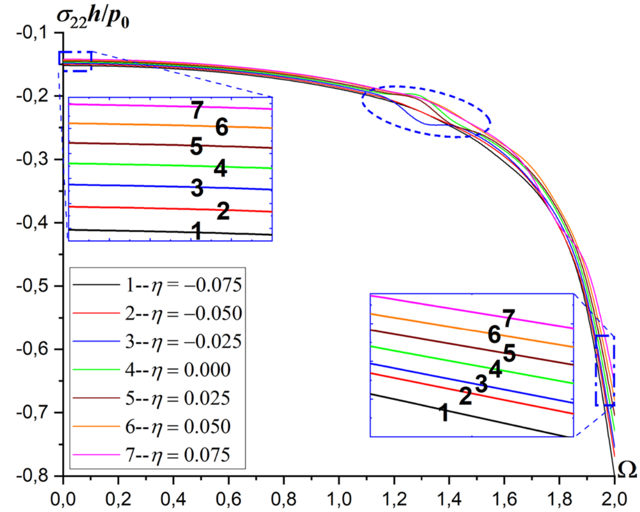

Fig. 11 Effect of the parameter η on the dependency between $\sigma_{22}h/p_0$ and Ω

the upper layer and the lower layer. In particular, PZT - 4 has more capability of stress isolation than $BaTiO_3$ and in this context, PZT - 4 might be a better choice for a material designation.

Figure 9 shows the interaction between $\sigma_{22}h/p_0$ and Ω for various values of the ratio h_P. Here, the changing parameter is the height of the plate for fixed values of other dimensions. It is seen that increasing the plate's thickness causes a decrease in the absolute values of the stress $\sigma_{22}h/p_0$. Besides, the ratio h_P shifts the resonance value $\Omega*$ to the right-hand side. This means that the ratio h_P exceeds the resonance mode of $\sigma_{22}h/p_0$. This is explained by the fact that when the ratio h_P increases, the stresses in the medium come into contact with more material particles, raising vibrations in the medium. As $\Omega \to \Omega*$, the oscillations of the graphs become more frequent. It is concluded from the graphs that the number of local peak points of the stress $\sigma_{22}h/p_0$ decreases cordially with h_P. It is evaluated from both Figs. 8 and 9 that the relationship between $\sigma_{22}h/p_0$ and Ω is non-monotonous. Considering both the consecutive stress values and all the given results here, it can be said that there is a direct link between $\sigma_{22}h/p_0$ and h_P has a direct link for $\Omega < \Omega*$. This is in good agreement with the one in Fig. 5. But, after $\Omega > \Omega*$, the mentioned link becomes unstable. So the ratio h_P has a great effect on the frequency response of the plate, in both qualitative and quantitative senses. Although the system has become more stable as h_P decreases, the total intrinsic stress in the system also increases. It is therefore useful to set a reasonable ratio h_P when designing the system under consideration.

Figure 10 illustrates the influence of the aspect ratio a on the dependency between $\sigma_{22}h/p_0$ and Ω. Herein, while a_1 is kept fixed, a_3 is changed. The values of $\Omega*$ decrease as the ratio a increases. This means that there is a destabilizing effect of increasing the ratio a. The influence of the external dynamic force on the frequency response of the piezoelectric plate increases in coordination with the ratio a. Further, the amplitudes of the resonance $\Omega*$ decrease considerably with the ratio a. In a nutshell, all the results prove that the resonance mode of the plate in response to the dynamic force depends quantitatively and qualitatively on the influence of the ratio a. It is a common result from Figs. 9 and 10 that increasing the dimensions of the piezoelectric plate prevents the resonance mode of the system, but the absolute values of the stress $\sigma_{22}h/p_0$ decrease. Compared to Figs. 9 and 10, it is seen that the effect of h_P on the resonance value $\Omega*$ is greater than that of a. When the vertical dimension of the plate increases (remember that the plate is polarized in the vertical direction), the electrical response of the plate in response to the dynamic force increases. This yields more vibrations in the medium. For more favorable values of these parameters, the piezoelectric plate can develop a more stable resonance case in any of the lower spatial vibrational modes.

The frequency response of the piezoelectric system subjected to the time-harmonic force is investigated in Fig. 11 by giving attention to the effect of the initial stress parameter η. Similar to Fig. 7, increasing the initial tension η^+ causes a decrease in the value of the stress $\sigma_{22}h/p_0$ but increasing initial compression η^- conversely increases the values of $\sigma_{22}h/p_0$. According to the oscillations of the graphs, static initial tension shifts the resonance domain forward while static initial compression encourages this domain. This means that the initial stress prevents the resonance values of the stress $\sigma_{22}h/p_0$. From this, it can be said that higher initial compression η^- could crash the system but higher initial tension η^+ becomes a more stable system. This is

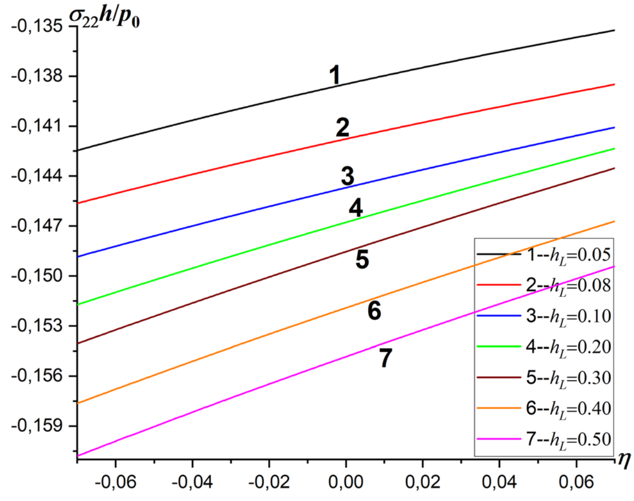

Fig. 12 Effect of the ratio h_P on the dependency between $\sigma_{22}h/p_0$ and η

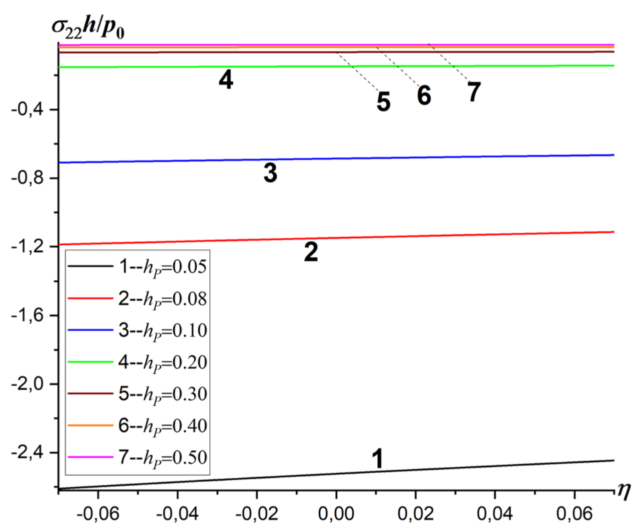

Fig. 13 Effect of the ratio h_P on the dependency between $\sigma_{22}h/p_0$ and η

explained in such that initial tension η^+ moves the particles of the object away from each other, absorbing the stress flow between them as much as possible while initial compression η^- brings the particles closer to each other, contributing to the stress flow between them. Frankly, the initial tension η^+ and initial compression η^- have opposite effects regarding the frequency response of the plate. All the results show that an initial stress case is a powerful tool for designing the bi-layered plate. In addition, it is noteworthy that there are local parametric resonance domains produced by the parameter η.

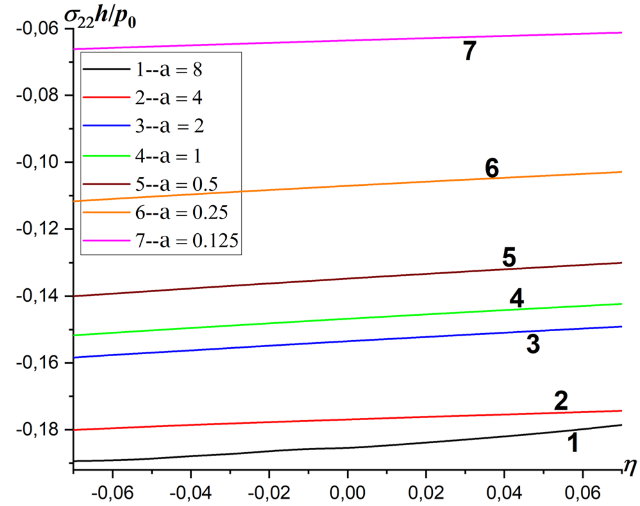

Fig. 14 Effect of the ratio a on the dependency between $\sigma_{22}h/p_0$ and η

This is marked as a blue-dashed ellipse. It is evaluated that there is an indirect link between the initial stress state and the resonance mode of the plate. As a result, the initial stress parameter η is of significant influence, in both the quantitative sense and the qualitative sense.

Now, let us focus on the dependency between $\sigma_{22}h/p_0$ and η for certain values of various geometrical factors. In Fig. 12, the relationships between $\sigma_{22}h/p_0$ and η for certain values of the ratio h_L. Further, Fig. 13 displays the influence of the ratio h_P on the dependency between $\sigma_{22}h/p_0$ and η while Fig. 14 provides the influence of the ratio a on the mentioned dependency.

It is a common result from Figs. 12, 13 and 14 that the stress $\sigma_{22}h/p_0$ changes linearly versus the parameter η. The slope of each graph increases cordially with the ratio h_L. This means that the influence of the static initial stress state on the dynamic response of the plate increases with h_L. The result is explained by the fact that the particles of $BaTiO_3$ have more talent mirroring the mentioned effect on the dynamic response by the external force of the plate than the ones of PZT - 4. Unlike other geometrical parameters, the ratio h_P has a lower influence on the dependency between $\sigma_{22}h/p_0$ and η. As h_P increases, the influence of the initial stress parameter η on the stress $\sigma_{22}h/p_0$ decreases. Accordingly, as the height of the plate increases, although the surface where is applied to initial stress grows up, the stress $\sigma_{22}h/p_0$ converges asymptotically to a particular value, the influence of the parameter η on the dynamic response of the plate decreases. In addition, the influence of the parameter η on the mentioned dynamic response increases with the ratio a. Increasing the plate sizes in the directions in which the normal initial stress force is applied leads more particles to resist the stress wave caused by the dynamic force.

Conclusions

In this work, the dynamic response of the bi-layered piezoelectric plate with initial stresses subjected to a time-harmonic force, standing on a rigid foundation was investigated using the finite element method (FEM). According to the three-dimensional linearized theory of elasticity for solids under initial stress (TLTESIS), the equations of motion and the related boundary-contact conditions were derived within the scope of the piecewise homogeneous body model. The FEM formulation was derived using the fundamental principle of total potential energy in view of the variational calculus and the linear coupled constitutive equations of the piezoelectric medium. Next, a PC algorithm was created to observe the plate's dynamic behavior. Next, the validity and trustiness of the numerical results were proven beyond any doubt and some numerical discussion and findings were presented. The following are some of the main numerical observations:

- While the ratio h_L and the parameter η have a limited effect on the dynamic response of the system, the ratios a and h_P have a direct effect;
- while the initial compression state encourages the resonance mode of the system, the initial tensile prevents that mode;
- when the system is designed, the selection of materials is an important issue since the stress transition across the interface is quite sensitive with the reason for the electrical response in addition to the mechanical one;
- and an increase in the values of the geometrical parameters of the problem prevents the effect of the initial stress state on the dynamic response of the plate.

Acknowledgements We express our deep thanks to the anonymous referees for their valuable comments and contributions on the earlier version of this paper.

Funding Open access funding provided by the Scientific and Technological Research Council of Türkiye (TÜBİTAK).

Data availability The datasets generated during and/or analyzed during the current study are available from the corresponding author upon reasonable request.

Declarations

Conflict of interest The author declares no potential conflicts of interest with respect to the research, authorship, and/or publication of this article.

References

1. Yang J (2005) An introduction to the theory of piezoelectricity. Springer, New York
2. Tiersten HF (2013) Linear piezoelectric plate vibrations: elements of the linear theory of piezoelectricity and the vibrations piezoelectric plates. Springer
3. Nguyen DD (2014) Nonlinear static and dynamic stability of functionally graded plates and shells. Vietnam National University Press, Hanoi
4. Southwell RV (1914) V. On the general theory of elastic stability. Philos Trans R Soc Ser A 213:187–244
5. Biezeno CB, Hencky H (1928) On the general theory of elastic stability. Proc Koninklijke Nederlandse Akademie van Wetenschappen 31:569–592
6. Biot MA (1939) Nonlinear theory of elasticity and the linearized case for a body under initial stress. Philos Mag Ser 7(27):468–489
7. Neuber H (1943) Die Grundgleichungen der elastischen Stabilität in allgemeinen Koordinaten und ihre Integration. ZAMM J Appl Math Mech 23(6):321–330
8. Green AE, Rivlin RS, Shield RT (1952) General theory of small deformations superposed on large elastic deformations. Proc R Soc A 211:211–292
9. Guz AN (1972) Three-dimensional theory of elastic stability under finite subcritical deformations. Soviet Appl Mech 8:1308–1323
10. Tiersten HF (1978) Perturbation theory for linear electroelastic equations for small fields superposed on a bias. J Acoust Soc Am 64(3):832–837
11. Hoger A (1986) On the determination of residual stress in an elastic body. J Elast 16(3):303–324
12. Ogden RW (1997) Non-linear elastic deformations. Ellis Horwood/Halsted Press, New York
13. Reddy JN (2003) Mechanics of laminated composite plates and shells: theory and analysis. CRC Press
14. Wang HM, Zhao ZC (2013) Love waves in a two-layered piezoelectric/elastic composite plate with an imperfect interface. Arch Appl Mech 83:43–51
15. Yu J, Zhang C (2014) Effects of initial stress on guided waves in orthotropic functionally graded plates. Appl Math Model 38(2):464–478
16. Rouzegar J, Abad F (2015) Free vibration analysis of FG plate with piezoelectric layers using four-variable refined plate theory. Thin-Walled Struct 89:76–83
17. Kurt I, Akbarov SD, Sezer S (2016) The influence of the initial stresses on Lamb wave dispersion in pre-stressed PZT/Metal/PZT sandwich plates. Struct Eng Mech 58(2):347–378
18. Daşdemir A (2017) Effect of imperfect bonding on the dynamic response of a pre-stressed sandwich plate-strip with elastic layers and a piezoelectric core. Acta Mech Solida Sin 30:658–667
19. Nguyen DD (2018) Nonlinear thermo-electro-mechanical dynamic response of shear deformable piezoelectric sigmoid functionally graded sandwich circular cylindrical shells on elastic foundations. J Sandwich Struct Mater 20(3):351–378

20. Kumar R, Singh K, Pathania DS (2019) Shear waves propagation in an initially stressed piezoelectric layer imperfectly bonded over a micropolar elastic half space. Struct Eng Mech 69(2):121–129
21. Kumar P, Mahanty M, Chattopadhyay A, Singh AK (2019) Effect of interfacial imperfection on shear wave propagation in a piezoelectric composite structure: Wentzel–Kramers–Brillouin asymptotic approach. J Intell Mater Syst Struct 30(18–19):2789–2807
22. Shahdadi A, Rahnama H (2020) Free vibration of a functionally graded annular sector plate integrated with piezoelectric layers. Appl Math Model 79:341–361
23. Chan DQ, Thanh NV, Khoa ND, Duc ND (2020) Nonlinear dynamic analysis of piezoelectric functionally graded porous truncated conical panel in thermal environments. Thin-Walled Struct 154:106837
24. Sahu SA, Nirwal S, Mondal S (2021) Reflection and transmission of quasi-plane waves at the interface of piezoelectric semiconductors with initial stresses. Appl Math Mech 42(7):951–968
25. Pankov AA (2022) Effect of the initial stress state on the effective properties of piezocomposite. Mech Compos Mater 58(5):733–746
26. Othmani C, Khelfa T (2023) Effect of graded pre-stress on the propagation of guided waves in functionally graded piezoelectric–piezomagnetic materials. Mech Res Commun 127:104037
27. Guz AN (2013) Fundamentals of the three-dimensional theory of stability of deformable bodies. Springer, New York (**Translated from Russian by M. Kashtalian**)
28. Akbarov SD (2015) Dynamics of pre-strained bi-material elastic systems: linearized three-dimensional approach. Springer, New York
29. Ilhan N (2012) The critical speed of a moving time-harmonic load acting on a system consisting a pre-stressed orthotropic covering layer and a pre-stressed half-plane. Appl Math Model 36(8):3663–3672
30. Negin M, Akbarov SD, Erguven ME (2014) Generalized Rayleigh wave dispersion analysis in a pre-stressed elastic stratified half-space with imperfectly bonded interfaces. Comput Mater Continua 42(1):25–61
31. Daşdemir A, Eröz M (2015) Mathematical modeling of dynamical stress field problem for a pre-stressed bi-layered plate-strip. Bull Malays Math Sci Soc 38(2):733–760
32. Yesil UB (2017) Forced and natural vibrations of an orthotropic pre-stressed rectangular plate with neighboring two cylindrical cavities. Comput Mater Continua 53(1):1–22
33. Glukhov AY (2018) Axisymmetric waves in prestressed incompressible laminated composite materials with sliding layers. Int Appl Mech 54(4):399–410
34. Daşdemir A (2020) Dynamic response of a bi-axially pre-stressed bi-layered plate resting on a rigid foundation under a harmonic force. Proc Inst Mech Eng C J Mech Eng Sci 234(3):784–795
35. Akbarov SD, Bagirov ET (2022) Dispersion of the axisymmetric waves propagating in the hydro-elastic system consisting of the pre-strained highly elastic plate, compressible inviscid fluid, and rigid wall. Arch Appl Mech 93:863–879
36. Tiersten HF (1969) Linear piezoelectric plate vibrations. Plenum, New York
37. Daşdemir A (2023) Effect of interaction between polarization direction and inclined force on the dynamic stability of a pre-stressed piezoelectric plate. Mech Res Commun 131:104150
38. Petyt M (2010) Introduction to finite element vibration analysis. Cambridge University Press, New York
39. Topolov VY, Bowen CR (2009) Electromechanical properties in composites based on ferroelectrics. Springer, London
40. Uflyand YaS (1967) Integral transformations in the theory of elasticity. Nauka, Moscow-Leningrad (**in Russian**)
41. Akbarov SD, Ilhan N (2013) Time-harmonic Lamb's problem for a system comprising a piezoelectric layer and piezoelectric half-plane. J Sound Vib 332(21):5375–5392
42. Daşdemir A, Eröz M (2019) Forced vibration of a bi-axially pre-stressed plate subjected to a harmonic point force and resting on a rigid foundation. Trans Can Soc Mech Eng 43(3):333–343
43. Daşdemir A (2022) A modal analysis of forced vibration of a piezoelectric plate with initial stress by the finite-element simulation. Mech Compos Mater 58(1):69–80
44. Timoshenko S, Godier JN (1951) Theory of elasticity. McGraw Hill, New York